Modeling of Protein Interactions Involved in Cardiac Tension Development

FB Sachse, KG Glänzel, G Seemann

Institut für Biomedizinische Technik, Universität Karlsruhe (TH),
Karlsruhe, Germany

Abstract

Modeling of protein interactions responsible for cardiac tension development can enhance the understanding of physiological and pathophysiological phenomena of the heart. Principal components of muscular tension development are the proteins actin, myosin, troponin, and tropomyosin. The tension is produced by cross-bridge cycling of actin and myosin using adenosine triphosphate as energy source. The cross-bridge cycling is initiated by binding of intracellular calcium to troponin and resulting configuration changes of tropomyosin.

In this work a hybrid model of protein interactions in cardiac tension development is derived on basis of recent measurements and descriptions on protein level. Dependencies on intracellular calcium concentration, sarcomere stretch, and stretch velocity as well as cooperativity mechanisms are incorporated. The model quantifies the tension development by states associated to configurations of the involved proteins. The model enables in conjunction with electrophysiological models of cardiac myocytes the reconstruction of electro-mechanical phenomena. Numerical simulations with the hybrid model were performed, which illustrated the reconstruction of steady state and length switches experiments. The steady state experiments describe the force-cytosolic $[Ca^{2+}]$ relationship in intact rat cardiac trabeculae. The length switch experiments provide data on the redevelopment of force after sudden stretch in rabbit right ventricular papillary muscles. Results of the numerical simulations show quantitative agreement with experimental studies.

The hybrid model of cardiac tension development offers interfaces to further models of cardiac electro-mechanics. The hybrid model can be coupled with models of cellular electrophysiology and passive mechanics of myocardium allowing the inclusion of mechano-electrical feedback mechanisms. The hybrid model can be applied to elucidate cooperativity mechanisms, pathophysiological changes, and metabolism of tension development.

1. Introduction

Muscles and the comprising myocytes are not only passively reacting to external forces, but can create internal tension resulting in deformation and movement. Some first, out-dated theories explained these internal creation of tensions by folding or coiling of long protein filaments, e.g. the lactid acid theory. Experimental evidence for a different mechanism achieved by different microscopic techniques lead to the theories of sliding filaments [Huxley, 1957, Huxley, 2001], which were proposed in the year 1953 by A. F. Huxley and N. Niedergerke as well as H. E. Huxley and J. Janson.

The sliding filament theory was subsequently confirmed by a multitude of experiments. E.g. it was found by microscopy that whilst sarcomere contraction, i.e. the distance between the Z disks is decreased, the length of actin and myosin filaments is kept constant. Enhancements of the theory are resulting from improvements of measurement techniques and modeling approaches. Despite many parts of the tension development are clarified as far as to the molecular level, some details are still under exploration.

Responsible structures for the sliding of myofilaments are different proteins, particularly actin, myosin, troponin, and tropomyosin, arranged in the sarcomeres of myocytes [Bers, 1991]. The interplay of these proteins is enabled by different reversible chemical reactions primarily controlled by electrophysiological processes and metabolism.

In this work a hybrid model of cardiac tension development is derived from measurements and descriptions of the protein interactions. Modeling of these protein interactions provides knowledge of basic mechanisms and can enhance the understanding of physiological and pathophysiological cardiac phenomena [Sachse, 2002]. The model takes into account recent findings of protein structure and interactions. The model offers interfaces to electrophysiologic models of cardiac myocytes unifying common components. Simulations with the hybrid model and a further model explore the reconstructability of force measurements in studies of myocardium.

2. Mechanisms

2.1. Myosin

The members of the myosin family are so-called motor proteins, which transform chemically bound energy to mechanical energy [Lodish et al., 2001]. Members of the myosin family drive not only muscle contraction, but also intracellular transport processes, cytokinesis, and cell locomotion. Thirteen types of myosin are distinguished by genome analysis, e.g. myosin I, myosin II, and myosin V, which are found in eukaryotic cells. In contraction of cardiac, skeletal and smooth muscle the myosin II is involved. However, the mechanisms of energy transfer and mechanical behavior are similar in the different kinds of myosin.

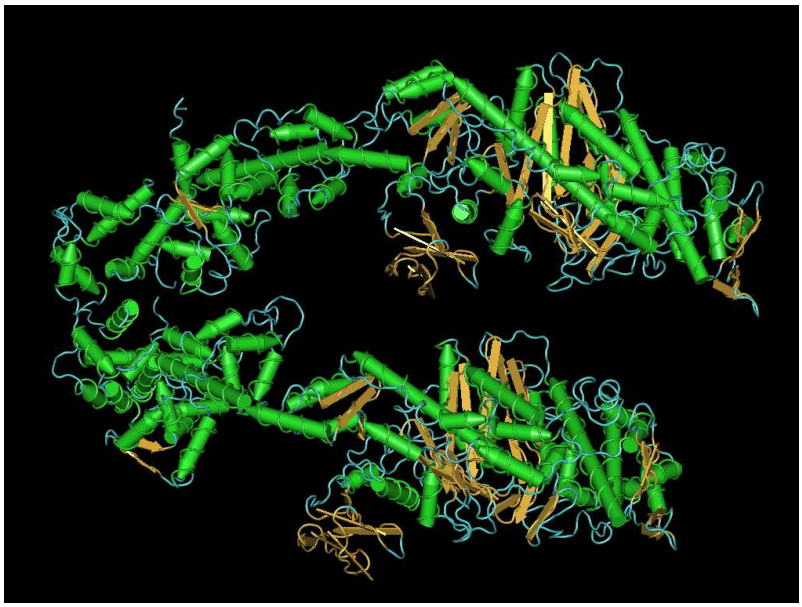

Figure 1. Molecular structure of myosin II (data from [Chen et al., 2002]). The protein can be divided in a head, neck and tail region. The chains of the head and neck region of species gallus gallus are visualized.

Energy source for myosin is adenosine triphosphate (ATP) produced in the mitochondria by oxygenation of nutrients and transferring its energy by hydrolysis. The hydrolysis consists of splitting the ATP into adenosine diphosphate (ADP), phosphate P_i, and the hydrogen ion H^+, whereby water H_2O is incorporated into the ATP:

$$\mathrm{ATP} + \mathrm{H_2O} \longrightarrow \mathrm{ADP} + \mathrm{P_i} + \mathrm{H^+} \tag{1}$$

The chemical reaction is conjuncted with a release of energy $\Delta G = -7.3 \frac{kcal}{mol}$, which is used to modify chemical bindings of myosin.

All kinds of myosin can be subdivided into a head, neck, and tail region (Fig. 1). Myosin II includes two pear-shaped heads showing binding sites for ATP and the protein actin. The neck region with a length of circa $8\ nm$ connects the heads with the two tails. The tails are coiled coil molecules.

2.2. Myofilaments in sarcomeres

The myofilaments in the sarcomeres are composed of so-called actin (thin) and myosin (thick) filaments [Bers, 1991] (Fig. 2). The thin filaments lead from the Z disks approximately $1\ \mu m$ towards the center of the sarcomere. The arrangement of thin filaments is thought to be maintained by the protein nebulin [Lodish et al., 2001].

The backbone of thin filaments is built up by two actin helices twined with concatenated long, flexible, coiled coil molecules, i.e. tropomyosin. Monomer actin, so-called G-actin, is a plate-shaped protein with a molecular weight of $42\ kD$ and a size of approximately $5,5\ nm \times 5,5\ nm \times 3,5\ nm$. G-actin polymerizes forming helices, so-called F-actin. In human six genes code the isoforms of actin, which is the most abundant protein in eukaryotic cells. Tropomyosin has a length of $40\ nm$ and possesses seven actin binding sites. One binding site is found for troponin. Commonly, seven actin molecules and one troponin molecule are attached to each tropomyosin.

Troponin consists of three components: troponin T, troponin I, and troponin C. Troponin T is connected to the tropomyosin and the two further components. Troponin I inhibits interactions between actin and myosin. Troponin C is of importance for the initiation of mechanical contraction by binding of calcium.

The thick filaments have a length of approximately $1.6\ \mu m$. They are arranged parallel to and between the thin filaments. The thick filament is composed primarily of the myosin molecule, which has a length of approximately $160\ nm$. A few hundreds of myosin molecules per thick filament are reported [Howard, 1997]. The thick filaments are bound via the protein titin to the Z disks [Lodish et al., 2001].

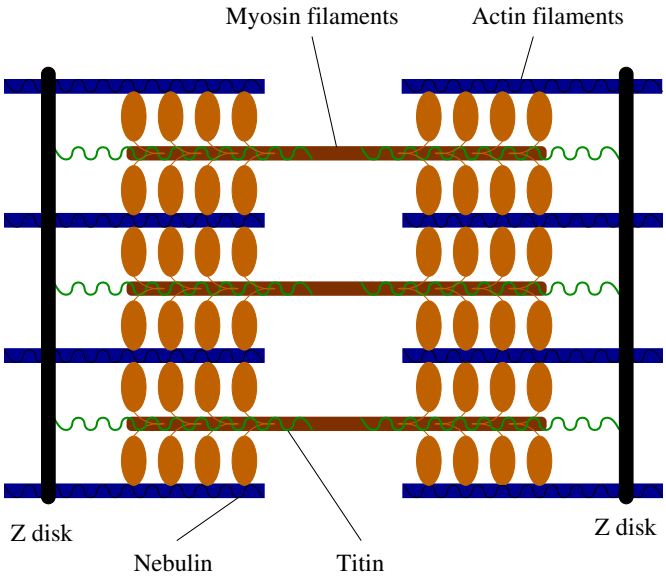

Figure 2. Schematic view of sarcomere (from [Sachse, 2002]). The sarcomere includes myofilaments, titin, and nebulin. Myofilaments are composed of actin and myosin filaments. The actin filaments, titin, and nebulin are attached to the Z disks, which border the sarcomere.

2.3. Intracellular calcium handling

The development of tension in the sarcomeres is provoked by an increase of the concentration of cytoplasmic calcium. Commonly, the increase of the concentration is result of electrical excitation. The concentration is affected primarily by sarcolemmal and sarcoplasmic proteins, which control the flow of calcium from and to spatial micro-domains within the cell [Bers, 2002].

The sarcolemmal Na-Ca exchangers and calcium pumps can remove calcium ions from the cytoplasm into the extracellular space. Voltage gated calcium ion channels allow the controlled influx of calcium. In mammalian myocytes a high density of Na-Ca exchangers and of L-type calcium ion channels is reported at the end of transversal tubuli, which intrude into the myocyte as a specialization of the sarcolemma and end at adjacencies of Z disks.

The intracellular calcium handling is carried out in large parts by the sarcoplasmic reticulum, which is decomposed in the terminal cisternae and longitudinal tubuli. The longitudinal tubuli surround mesh-like the sarcomeres. The terminal cisternae located at the Z disks act primarily as buffer for calcium resulting from a high density of the protein calsequestrin. The sarcoplasmic reticulum includes different proteins controlling the calcium flux through the membrane. Sarcoplasmic calcium pumps remove calcium ions from the cytoplasm into the sarcoplasmic reticulum consuming ATP. Sarcoplasmic calcium release channels are gated by cytoplasmic calcium concentration and allow the efflux of calcium from the junctional sarcoplasmic reticulum into the cytoplasm.

2.4. Excitation-contraction coupling

A physiological initiation of tension development is performed by electrical excitation of the myocyte. The excitation propagates over the sarcolemma, particularly the transversal tubuli, where in consequence the sarcolemmal voltage-gated L-type calcium ion channels open initiating a positive feed back mechanism. The influx of calcium ions through the L-type calcium ion channels triggers the opening of sarcoplasmic calcium release channels leading to calcium sparks. Numerous calcium sparks sum up to a significant increase of the concentration of cytoplasmic calcium. The release channels show a refractory period, which stops the positive feed back mechanism. The calcium is reuptaken by calcium specific pumps into the sarcoplasmic reticulum. Smaller amounts are transported extracellularly via the sarcolemmal Na-Ca exchangers and calcium pumps.

The calcium binds to troponin C resulting in structural changes of the troponin-tropomyosin-actin complex followed by shifting of the tropomyosin over the actin filament [Bers, 1991]. The changes allow the strong binding of a myosin head to

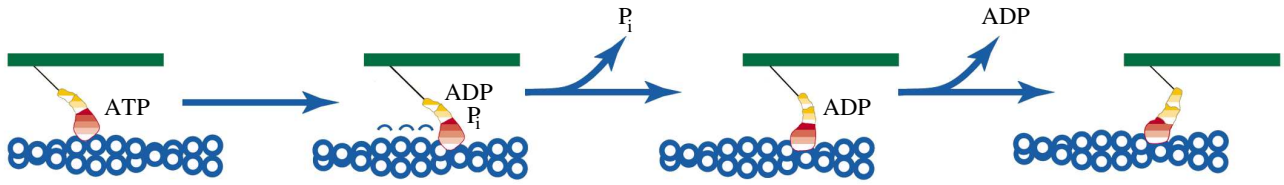

Figure 3. Sliding of myosin and actin filament (adapted from [Irving and Goldman, 1999]). The sliding starts with the binding of ATP to the myosin head, followed by its unbinding and rebinding to actin. The distance between the binding positions is a multiple of a minimal length. The ATP is hydrolyzed and the metabolites, P_i and ADP, are released sequentially into the cytoplasm. Between the second and third step a so-called power stroke is performed, developing tension and/or changing the relative position of the myofilaments. The illustrated processing presumes, that a formation of cross bridges of actin and myosin is possible. Commonly, structural changes of the troponin-tropomyosin-actin complex resulting from calcium binding to troponin C are necessary to allow the formation.

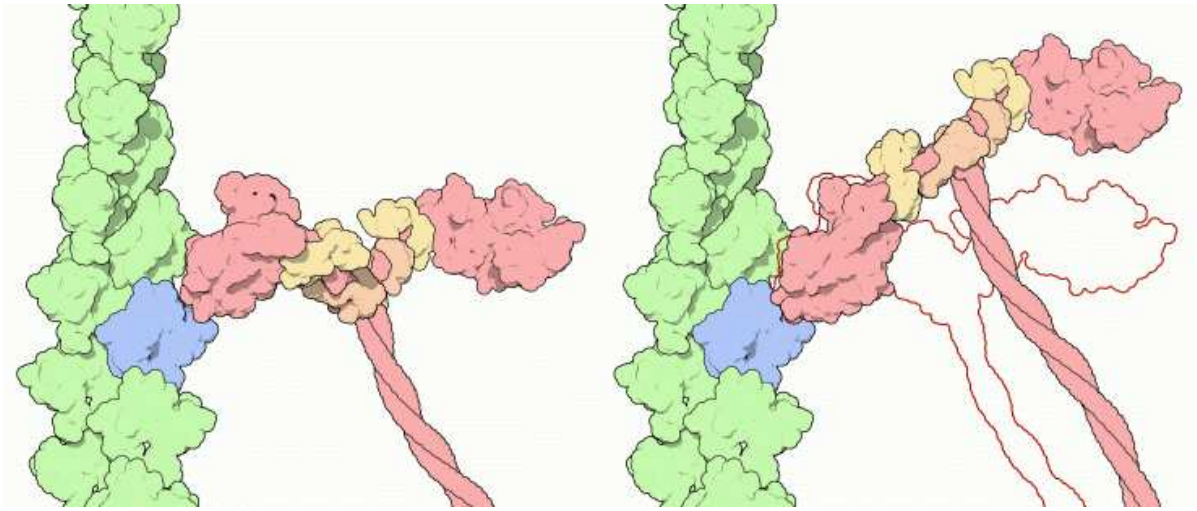

Figure 4. Attachment of actin to myosin and its folding (from [Goodsell, 2001]). The myosin head and tail is shown in red, its light chains in orange and yellow. The actin filament is visualized in green and blue. The left hand illustration shows a myosin head attached to actin, the right hand the folding of the myosin head.

actin, the so-called cycling of cross bridges or actin-activated myosin II ATPase cycle. In absence of ATP the actin-myosin binding is arrested. By binding and hydrolysis of ATP the motor protein performs four major steps (Fig. 3):

- Binding of ATP to myosin head resulting in its unbinding from actin
- Rebinding of myosin head at adjacent actin while ATP hydrolysis
- Changing of the angle of myosin heads to neck and tails (Fig. 4), whereby phosphate P_i is released into the cytoplasm
- Unbinding of ADP from myosin and its release into the cytoplasm

If the concentration of intracellular calcium and ATP is sufficiently large, the procedure is repeated.

A more detailed description of the actin-activated myosin II ATPase is given in Fig. 5, which shows states of myosin and reversible transitions. In further descriptions strong and weak binding of myosin to actin is distinguished [Gordon et al., 2001].

Different step lengths and tensions are reported for the variant types of myosin and myocytes. Step lengths, which are multiple of a minimal length, and back steps are reported in recent experimental works. These works change the deterministic view point to a stochastical.

For myosin II one up to five sub-steps per hydrolyzed ATP are performed by folding of the head-neck junction, whereby the multiple steps are still controversial and partly probably attributed to the measurement equipment [Irving and Goldman, 1999]. Each folding of myosin II leads to sub-steps with a length of circa $5.3\ nm$ in direction of the actin filament [Kitamura et al., 1999] and a summary force of $1 - 5\ pN$ [Lodish et al., 2001].

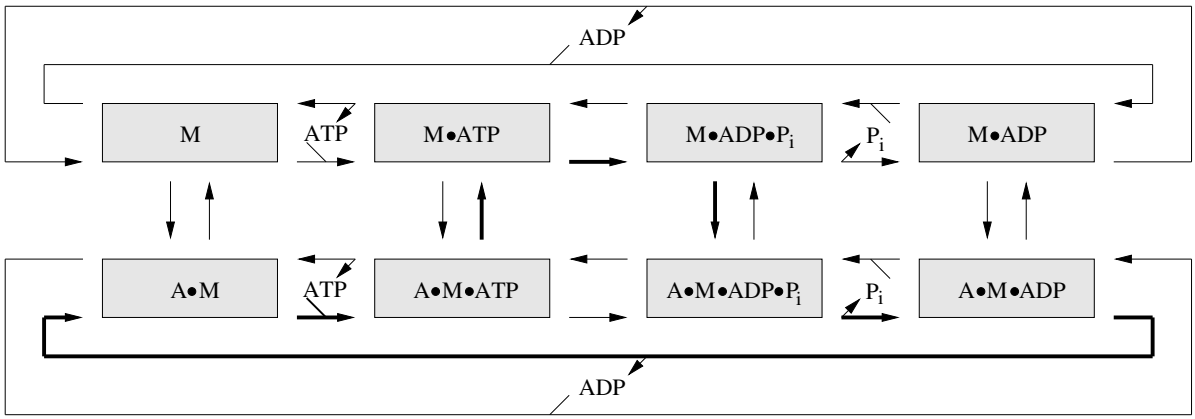

Figure 5. States and transitions of actin-activated myosin II ATPase cycle (adapted from [Bers, 1991, Spudich, 2001]). The quads symbolize the different states of myosin. M and A indicate myosin and actin, respectively. ATP, ADP, and P_i represent adenosine triphosphate, adenosine diphosphate, and phosphate, respectively. Arrows indicate possible transitions. The bold arrows signify the normal transitions.

A multitude of power strokes sum up during sarcomere's contraction and tension development. Several configuration changes of the involved proteins lead to a cooperativity of the tension development. Different cooperativity mechanisms for tension development are reported:

- calcium binding to troponin C increases affinity for binding of calcium to troponin C (TN-TN) [Gordon et al., 2001]
- cross-bridges increase affinity for binding of calcium to troponin C (XB-TN) [Allen and Kurihara, 1982]
- cross-bridges support the building of cross-bridges in the neighborhood (XB-XB) [Nagashima and Asakura, 1982, Swartz and Moss, 1992]
- shifting of tropomyosin leads to shifting of attached tropomyosins (TM-TM) [Moss et al., 1986, Tobacman, 1996]

3. Experimental studies

A large number of experiments of active muscular behavior was performed starting with experiments of A. V. Hill in 1938 [Hill, 1938], who measured, analyzed, and described in a mathematical manner the interdependencies between speed of shortening, tension, and heat production in skeletal muscles of frog. In these experiments the muscle load was varied. The muscle was clamped at both ends, its length was fixed and noted. The muscle was tetanized isometrically by electrical stimulation. After quick release of the fixation the muscle shortened and the shorting velocity was measured. The measurement data was used to parameterize an equation, which is now known as Hill's equation.

As for acquisition of passive mechanical properties the specimens for the measurement of active muscular behavior are primarily from the species rat, rabbit, and cat (tables 1 and 2). The size of specimens varies between large papillary muscles, differently shaped blocks of myocardial tissue, small cellular clusters of myocytes to single myocytes.

The development of tension in myocardial tissue and myocytes is measured with devices similar to those for acquisition of passive mechanical properties. In contrast thereto specific extensions are included in the devices to activate a tension development, e.g. indirectly by electrical stimuli or directly by an increase of the concentration of intracellular calcium $[Ca^{2+}]_i$. Miscellaneous macroscopic and microscopic measurement devices were applied to record the active mechanics. Commonly, the devices were specifically developed dependent on the specimens size and geometrical properties.

The early works involved in measurement of active mechanics of cardiac muscle followed the experimental and conceptual approaches of Hill. The relationships between tension, stretch, and stimulus frequency as well as the underlying mechanisms, e.g. electro-mechanic coupling, were focus of interest. The primary specimens used in the early works were ventricular trabeculae obtained after rapid removal of the heart. The specimens were suspended in an appropriate fluid. Electrical stimulation of the muscles was performed by applying current via electrodes. In further commonly used protocols the muscle length was constant over the whole measurement time or length switches were performed, which change the length of a muscle suddenly by given displacements [Parmley and Chuck, 1973, Peterson et al., 1991].

Already in early works, e.g. of Sonnenblick [Sonnenblick, 1964] and Parmley et al. [Parmley and Chuck, 1973], and similar to measurements of skeletal muscle a stretch dependence of the tensions developed in myocardium was reported. This

Tissue/Cell type	Species	Reference
papillary muscle	cat	[Sonnenblick, 1964]
papillary muscle	cat	[Parmley and Chuck, 1973]
papillary muscle	cat, rat	[Ingebretsen et al., 1976]
Purkinje fibers	sheep	[Eisner et al., 1984]
papillary muscle	ferret	[Wier and Yue, 1986]
intact and skinned trabeculae	rat	[Kentish et al., 1986]
skinned ventricular muscle bundles	cow	[Hofmann and Fuchs, 1987]
papillary muscle	New Zealand White rabbit	[Peterson et al., 1991]
ventricular myocardium	New Zealand White rabbit	[Nassar et al., 1991]
right ventricular papillary muscle	rabbit	[Bluhm and Lew, 1995]
divers	divers	[Wang and Patterson, 1995]
trabeculae	rat	[Janssen and Hunter, 1995]
trabeculae	rat	[Janssen and de Tombe, 1997]
ventricular muscle	rat	[Baker et al., 1998]
ventricular muscle	rat	[Maier et al., 1998]
papillary muscle	ferret	[Saeki et al., 1998]
skinned right ventricular trabeculae	rat, guinea pig	[Palmer and Kentish, 1998]
ventricular trabeculae	rat	[Layland and Kentish, 1999]
skinned ventricular fiber strips	rat	[Allen et al., 2000]
left ventricular papillary muscle	wild-type and phospholamban knockout mice	[Bluhm et al., 2000]
right atrial trabeculae fiber strips	human	[Maier et al., 2000]
right ventricular trabeculae	rat	[ter Keurs et al., 2000]
right ventricular trabeculae	rat	[Wannenburg et al., 2000]
skinned right ventricular trabeculae	rat	[Konhilas et al., 2002]

Table 1. Force measurements of cardiac muscle.

Myocyte type	Species	Reference
skinned ventricular	rat	[Fabiato and Fabiato, 1975]
-	rat	[de Clerck et al., 1977]
skinned ventricular	rabbit, frog, guinea pig, rat	[Bers, 1991]
ventricular	guinea-pig	[White et al., 1993]
ventricular	guinea-pig	[Gannier et al., 1993]
ventricular	guinea-pig	[White et al., 1995]
left ventricular	rabbit	[Bluhm et al., 1995]
skinned atrial and ventricular	frog	[Brandt et al., 1998]
left ventricular	canine	[O'Rourke et al., 1999]
ventricular	rat	[Yasuda et al., 2001]

Table 2. Force measurements of cardiac myocytes.

phenomenon can be regarded as the underlying principle of the Frank-Starling mechanism, which leads to an increase of contractile tension and ejection of blood by increase of the end-diastolic volume of the ventricular cavity. The phenomenon provides evidence for the sliding filament theory, whereby the overlapping of the myofilaments determines the recruitment and formation of cross bridges. The early works were validated by various subsequent experiments [ter Keurs et al., 2000]. E.g. it was found in experiments with constant or sinusoidally pertubated [Wannenburg et al., 2000] sarcomere length, that the overlap of the thick and thin filaments is a significant determinant of the force amplitude.

Careful observation revealed that the performing of length switches leads to transitions of tensions, which were time dependent [Parmley and Chuck, 1973]. E.g. a quick shortening to 90 % of the resting length leads an immediate decrease of force to circa 50 %. The subsequent transient rise of force by 10 % was followed by a slow asymptotic fall. The asymptotic force was 55 % of the force at resting length.

In further studies it was reported that the progression of tension is modulated by the progression of intracellular calcium

concentration $[Ca^{2+}]_i$. E.g. a graded effect of the intracellular calcium concentration $[Ca^{2+}]_i$ on the cross bridge kinetics was found in studies of chemically permeabilized ventricular trabeculae, whereby the calcium concentration was varied as well as the muscle length was sinusoidal pertubated [Wannenburg et al., 2000]. The regulation of the tension development kinetics by the extracellular calcium concentration $[Ca^{2+}]_i$ was reported in tetanized ventricular trabeculae [Baker et al., 1998]. Therefore, it can be concluded that also the progression of an electrical excitation influences the progression of the force development.

The relationship between tension and intracellular calcium is frequency dependent. Most studies with isolated myocardial preparations under physiologic conditions report a positive relationship, i.e. increasing the calcium frequency leads to higher tension [Layland and Kentish, 1999]. The positive relationship is attributed to a higher uptake of extracellular calcium into the myocyte by increasing stimulus frequency leading to a higher uptake and release of calcium in the sarcoplasmic reticulum. Under non-physiologic conditions the relationship can have a negative slope or show an U-shape as well as species and specimens dependent variations of the relationship were found [Saeki et al., 1998, Bluhm et al., 2000].

Variant measurements were performed with skinned myocytes, which permit directly the control of the environment inside of the cells. E.g. calcium can be applied into the intracellular space and to the contractile elements. A removal of sarcolemma can be achieved chemically as well as by mechanical homogenization and manual micro-dissection. A disadvantage of this kind of preparation is that cellular constituents may be lost, which affect the calcium sensitivity of myofilaments [Bers, 1991].

A classical work was carried out by Fabiato and Fabiato [Fabiato and Fabiato, 1975], who measured the tension of skinned myocytes and its interdependencies with calcium release and re-sequestrations by the sarcoplasmic reticulum. A single skinned myocyte was located in a perfusion chamber with the two ends of the cell attached to glass micro-needles. One micro-needle was fixed, the other connected to the lever of a force transducer. Force as well as length and width of the cell were measured. Furthermore, a mean sarcomere length was determined. Several conclusions were drawn from these measurements: Cellular tension is a direct effect of the concentration of free calcium, where the tension is developed regardless the deletion of the sarcoplasmic reticulum. A significant calcium sink exists in the cell, which was identified as the sarcoplasmic reticulum. Physiologically, calcium is re-sequestrated after contraction. The release of calcium from the sarcoplasmic reticulum is triggered by concentration of free calcium. The amplitude of contraction is increased when the triggering concentration of free calcium is increased.

Topic of recent studies are the effects of specific proteins and pathologies onto force and calcium handling. The role of the protein phospholamban, a inhibiting regulator of the sarcoplasmic calcium pump (SERCA), was studied with wild-type and phospholamban knockout mice [Bluhm et al., 2000]. The effects of hypertrophy and tachycardia were acquired in single myocytes as well as in myocardium [Maier et al., 1998, O'Rourke et al., 1999].

4. Modeling of cellular electrophysiology

Variant models of cellular electrophysiology were published in the last 40 years. In this work the Noble-Varghese-Kohl-Noble model was applied, which describes the electrophysiology of ventricular myocytes of guinea-pig (Fig. 6). The modeling of calcium handling includes the topics described in Sect. 2.3. The model reconstructs effects on ionic channels by the concentration of adenosine triphosphate and acetylcholine (ACh) as well as by stretching. Furthermore, a tension generation model is included. A description of the diadic space is incorporated. Different variants and configurations of the model exist. The variant applied in this work is based on [Noble et al., 1998, Kohl et al., 1998, Noble, 2000] neglecting ATP and ACh activated ionic channels as well as using only the electrophysiological part of the model.

The model includes dependencies of electrophysiological parameters on the length or tension of the sarcomere. The mechano-electric feedback is realized by introducing stretch-activated ion conductances, a modulation of calcium binding to troponin C, and a modulation of sarcoplasmic leak current. The usage of the mechanisms in the hybrid model presented in this work is restricted to the incorporation of length dependencies of the electrophysiological parameters. Stretch activated ion channels were deactivated.

5. Modeling of tension development

5.1. Overview

A first attempt to describe mathematically active tensions developed in muscle was published 1938 by A. V. Hill [Hill, 1938]. He developed the model on base of his work concerning heat production in striated muscle, wherefore he received a Nobel prize in 1922. The description refers to the force-velocity relationship of tetanized skeletal muscle of

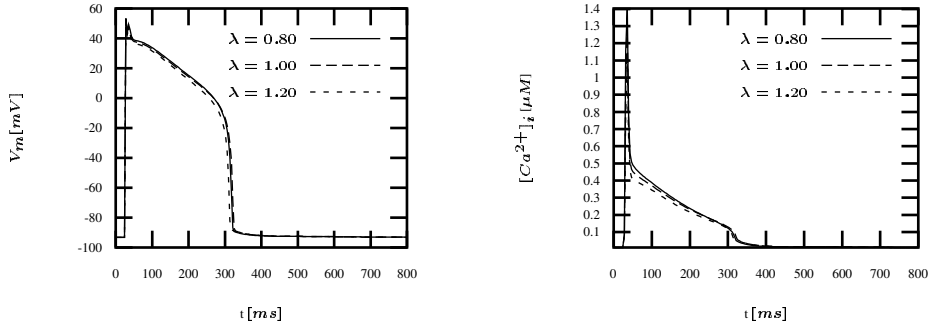

(a) (b)

Figure 6. Simulation of electrophysiology of ventricular myocytes of guinea-pig with variant of Noble-Varghese-Kohl-Noble model [Noble et al., 1998, Kohl et al., 1998, Noble, 2000]. (a) Transmembrane voltage and (b) intracellular calcium concentration $[Ca^{2+}]_i$ are reconstructed for different stretches λ. A stimulus current was applied at $t = 25\ ms$ to the electrophysiological model. Stretch activated ion channels were deactivated. The binding of intracellular calcium to troponin C and the sarcoplasmic leak current was modulated by stretch.

frog upon quick release from isometric condition. In the context of a mathematical modeling of the heart Hill's equation is primarily of pedagogical value, because the general framework is differing between the two muscle types. A tetanized contraction is physiologically not common for cardiac muscle. The coupling to electrophysiologic quantities is not included in Hill's equation but is of fundamental importance for cardiac tension development. Hill's equation can be regarded as an empirical equation [Fung, 1993], which gives macroscopic information and neglects biophysical phenomena on microscopic and molecular level.

Of special interest for biophysically motivated modeling are descriptions of cellular tension development, which base on electrophysiological parameters delivered e.g. by quantitative models of cellular electrophysiology. The concentration of intracellular calcium $[Ca^{2+}]_i$ is used to define rate coefficients, which depict the interaction between states of actin and myosin. The state variables describe e.g. the binding of intracellular Ca^{2+} to the troponin complex and the cross bridge cycling. Further parameters influencing the rate coefficients are the sarcomere length and the state variables.

Variant biophysically motivated models were generated in the last years describing force development [Sachse, 2002]. Commonly, these model describe force development by systems of coupled differential equations of first order. The complexity of these models increased over the last years, because more and more details of the process are accumulated. These details are elucidated by experiments, which allow a quantitative description. Particularly, quantitative data on protein interactions is now available.

5.2. Models of Rice et al.

Rice et al. described 5 models reproducing the tension development in cardiac muscle [Rice et al., 1999]. In this work the 3rd model is applied as basis the generation of the hybrid model and for comparison (Fig. 7). The model uses 6 state variables, $N0$, $N1$, $P0$, $P1$, T, and TCa with:

$$N0 + N1 + P0 + P1 = 1 \tag{2}$$

$$T + TCa = 1 \tag{3}$$

The state variables $N0$, $N1$, $P0$, and $P1$ describe the configuration of tropomyosin and the cross-bridge cycling, the state variables T and TCa the binding of intracellular calcium Ca^{2+} to troponin C and the resulting interaction between the troponin complex and tropomyosin. The interaction between the state variables of the model is described by a system of first

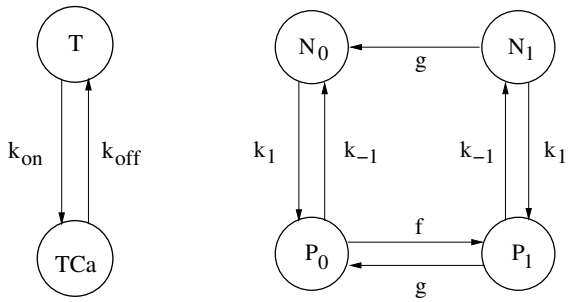

(a) (b)

Figure 7. State diagram of 3rd Rice-Winslow-Hunter model. (a) Two state variables quantify the calcium binding to troponin C. (b) Four state variables describe the configuration of tropomyosin and the cross-bridge cycling. The transition between states are depicted by arrows labeled with constants k_x, which are parameters of the rate coefficients functions.

order differential equations:

$$\frac{\partial}{\partial t}\begin{pmatrix} N0 \\ P0 \\ P1 \\ N1 \\ T \\ TCa \end{pmatrix} = \boldsymbol{R}\begin{pmatrix} N0 \\ P0 \\ P1 \\ N1 \\ T \\ TCa \end{pmatrix} \tag{4}$$

with the 6×6 matrix $\boldsymbol{R}$. The matrix $\boldsymbol{R}$ consists of rate coefficients:

$$\boldsymbol{R} = \begin{pmatrix} -k_1\left(SL,[Ca^{2+}]_i\right) & k_{-1} & 0 & g & 0 & 0 \\ k_1\left(SL,[Ca^{2+}]_i\right) & -k_{-1}-f & g & 0 & 0 & 0 \\ 0 & f & k_{-1}-g & k_1\left(SL,[Ca^{2+}]_i\right) & 0 & 0 \\ 0 & 0 & k_{-1} & -k_1\left(SL,[Ca^{2+}]_i\right)-g & 0 & 0 \\ 0 & 0 & 0 & 0 & -k_{on}[Ca^{2+}]_i & k_{off} \\ 0 & 0 & 0 & 0 & k_{on}[Ca^{2+}]_i & -k_{off} \end{pmatrix} \tag{5}$$

The coefficients k_{on}, k_{off}, f, g, and k_{-1} are constants. The rate coefficient k_1 is a function of the sarcomere length SL and the concentration of intracellular calcium $[Ca^{2+}]_i$.

The normalized force F is determined by

$$F = \frac{\alpha(P1+N1)}{F_{max}} \tag{6}$$

with the sarcomere overlap function $\alpha = \alpha(SL)$ (Fig. 8) and the maximal force F_{max}. The state variables $P1$ and $N1$ quantify the force generating states.

5.3. Hybrid model

The hybrid model combines a description of the binding of intracellular calcium $[Ca^{2+}]_i$ to troponin C, the configuration change of tropomyosin, and the interaction of actin and myosin [Glänzel, 2002]. The calcium binding to troponin C is similarly described as in the 3rd Rice-Winslow-Hunter model [Rice et al., 1999]. The interaction of actin and myosin is adopted from Gordon et al. [Gordon et al., 2001], Bers et al. [Bers, 1991], and Spudich [Spudich, 2001]. The cooperativity mechanisms XB-TN, XB-XB, and TM-TM are incorporated in the hybrid model. The model uses as input the concentration of intracellular calcium $[Ca^{2+}]_i$, the sarcomere stretch λ, and the sarcomere stretch velocity v. As alternative to the intracellular calcium $[Ca^{2+}]_i$ the calcium bound to troponin C can be provided as input. The model delivers as output a normalized tension and optionally the intracellular calcium $[Ca^{2+}]_i$ modified by calcium bound to troponin C.

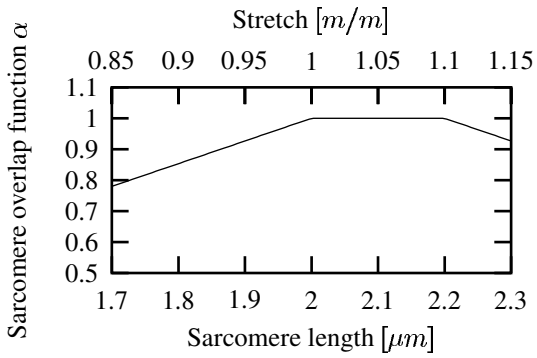

Figure 8. Sarcomere overlap function (data from [Rice et al., 1999]). The function quantifies the fraction of myosin heads that are capable to interact with actin in such a way that force is produced. The overlap function is dependent on stretch. The scaling of the lower axis assumes a default sarcomere length of 2 μm.

The model uses 14 state variables, which are coupled by rate coefficients. Two state variables, T and TCa, detail the binding of intracellular calcium Ca^{2+} to troponin C (Fig. 9a). The state variable T describes the normalized concentration of troponin C with no bound calcium, TCa the normalized concentration of troponin C with bound calcium. The normalization leads to:

$$T + TCa = 1 \tag{7}$$

Two further state variables, TM_{on} and TM_{off}, quantify the configuration of tropomyosin (Fig. 9b). The state variable TM_{on} describes the concentration of tropomyosin in permissive configuration, TM_{off} the normalized concentration in non permissive. The normalization leads to:

$$TM_{on} + TM_{off} = 1 \tag{8}$$

Ten state variables are used to quantify the interaction between actin and myosin, particularly the cross-bridge cycling (Fig. 9c). The ten variables describe normalized concentrations of myosin. The condition, that the variables sum up to 1, is used as normalization:

$$M \bullet ATP + M \bullet ADP \bullet P_i + M \bullet ADP + M \tag{9}$$

$$+A \sim M \bullet ATP + A \sim M \bullet ADP \bullet P_i \tag{10}$$

$$+A \bullet M \bullet ADP \bullet P_i + A \bullet M^* \bullet ADP + A \bullet M \bullet ADP + A \bullet M \quad = \quad 1 \tag{11}$$

The power stroke is performed during transition from $A \bullet M \bullet ADP \bullet P_i$ to $A \bullet M^* \bullet ADP$. The normalized concentration of myosin strongly bound to actin $S_{A \bullet M}$ is quantified by:

$$S_{A \bullet M} = A \bullet M \bullet ADP \bullet P_i + A \bullet M^* \bullet ADP + A \bullet M \bullet ADP + A \bullet M \tag{12}$$

The interaction between the states of the model is described by a system of first order differential equations:

$$\frac{\partial}{\partial t} \begin{pmatrix} T \\ TCa \\ TM_{off} \\ TM_{on} \\ M \bullet ATP \\ M \bullet ADP \bullet P_i \\ A \sim M \bullet ADP \bullet P_i \\ A \bullet M \bullet ADP \bullet P_i \\ A \bullet M^* \bullet ADP \\ A \bullet M \bullet ADP \\ A \bullet M \\ A \sim M \bullet ATP \\ M \\ M \bullet ADP \end{pmatrix} = \boldsymbol{R} \begin{pmatrix} T \\ TCa \\ TM_{off} \\ TM_{on} \\ M \bullet ATP \\ M \bullet ADP \bullet P_i \\ A \sim M \bullet ADP \bullet P_i \\ A \bullet M \bullet ADP \bullet P_i \\ A \bullet M^* \bullet ADP \\ A \bullet M \bullet ADP \\ A \bullet M \\ A \sim M \bullet ATP \\ M \\ M \bullet ADP \end{pmatrix} \tag{13}$$

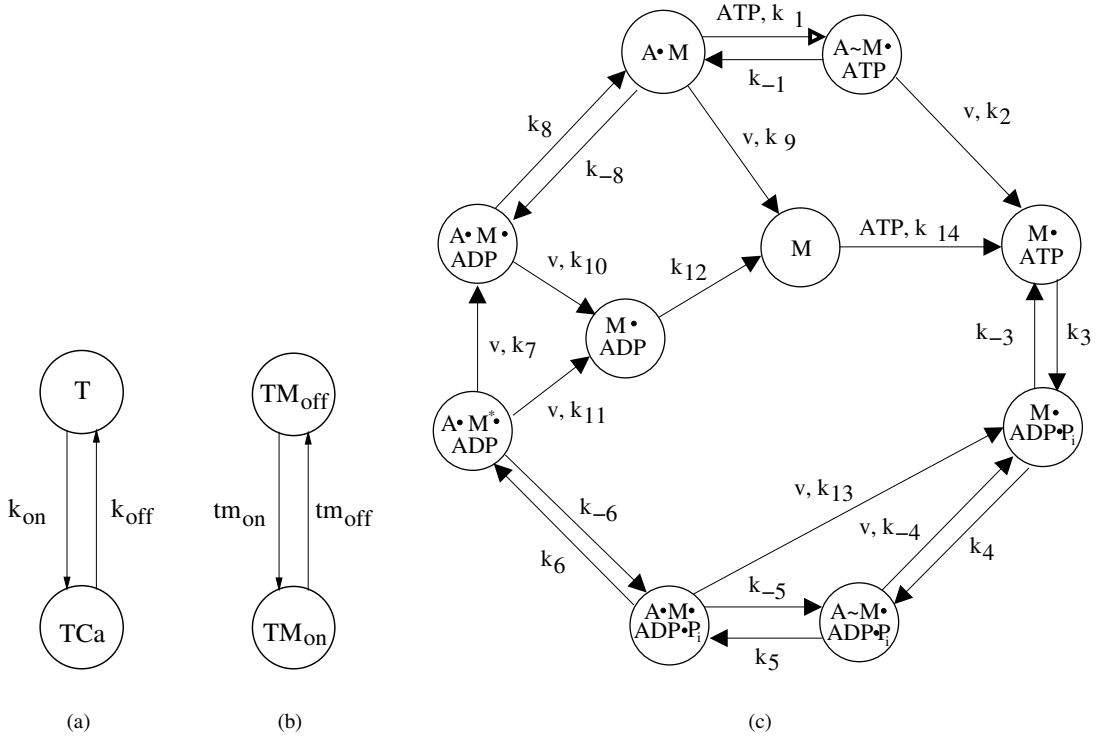

Figure 9. State diagram of hybrid model. (a) Two state variables quantify the calcium binding to troponin C. (b) Two further state variables describe the configuration of tropomyosin. (c) Ten state variables detail the interaction of actin and myosin as well as the hydrolysis of adenosine triphosphate. M and A symbolize myosin and actin, respectively. ATP, ADP, and P_i represent adenosine triphosphate, adenosine diphosphate, and phosphate, respectively. The transition between states is depicted by an arrow, strong binding by a closed circle, and weak binding by a tilde. The arrows are labeled with constants k_x, ATP, and stretch velocity v, which are parameters of the rate coefficients functions.

with the 14×14 matrix $\boldsymbol{R}$ consisting of rate coefficients. Partly, the rate coefficients are dependent on the sarcomere stretch velocity v, the sarcomere stretch λ, and the concentration of intracellular calcium $[Ca^{2+}]_i$. The matrix $\boldsymbol{R}$ is sparse indicating that transitions between states are only partly possible. The initial values and coefficients are given in the appendix 8.1.

The sum of tension generating states T_{AM} is given by:

$$T_{AM} = A \bullet M + A \bullet M \bullet ADP + A \bullet M^* \bullet ADP \tag{14}$$

The normalized force F is determined by

$$F = \frac{\alpha \, T_{AM}}{F_{max}} \tag{15}$$

with the sarcomere overlap function $\alpha = \alpha(\lambda)$ (Fig. 8), which is tissue and species specific [Bers, 1991, Rice et al., 1999], and maximal tension F_{max}, which is dependent on the rate coefficients. The normalized force F can be multiplied by a tissue and species specific factor f_{T0} to quantify force development of myocardium.

6. Results

6.1. Simulation of steady-state experiments

Steady state experiments show the influence of static stretch and static concentration of intracellular calcium $[Ca^{2+}]_i$ on the developed tension. Numerical simulations with the 3rd Rice-Winslow-Hunter and the hybrid model were performed

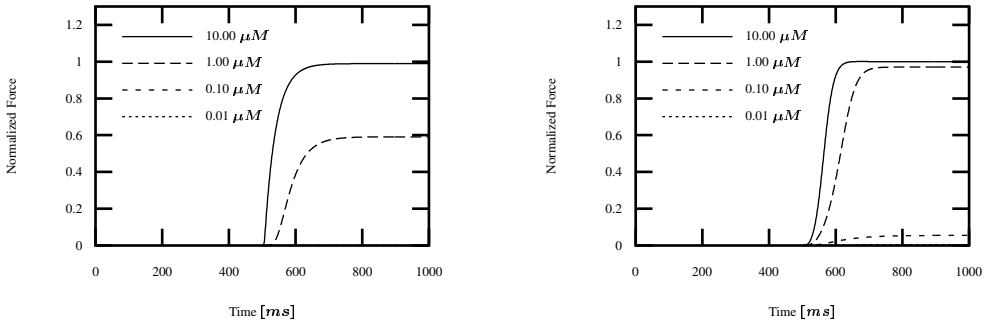

(a) (b)

Figure 10. Normalized force in dependency of concentration of intracellular calcium $[Ca^{2+}]_i$. In the simulations the concentration of intracellular calcium was set for 500 ms to 0 μM. For the next 500 ms the concentration was set to 0.01, 0.1, 1, or 10 μM. This raise results in an development of normalized force shown here for (a) 3rd Rice-Winslow-Hunter model [Rice et al., 1999] and (b) hybrid model. After a transient phase a constant, concentration dependent plateau was reached. The assigned normalized force was used for further evaluation.

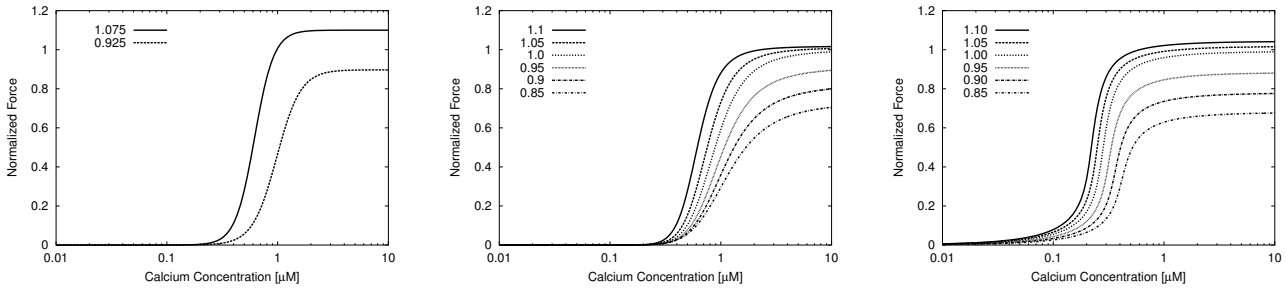

(a) (b) (c)

Figure 11. Normalized force in dependency of steady stretch and concentration of intracellular calcium $[Ca^{2+}]_i$. (a) Experimental data from ter Keurs et al. (adapted from [ter Keurs et al., 2000]) with stretch of 1.075 and 0.925 corresponding to a sarcomere length of 2.15 and 1.85 μm, respectively. (b) 3rd Rice-Winslow-Hunter model [Rice et al., 1999] and (c) hybrid model with a stretch varying from 0.85 to 1.1.

to reconstruct the measurements described in [ter Keurs et al., 2000], who investigated the steady state interdependencies between sarcomere length, intracellular calcium $[Ca^{2+}]_i$, and tension in right ventricular trabeculae of rat. Results of the experimental study are given in Fig. 11 a. For two measurements with different sarcomere length a function is shown, which approximates the measured data using a Hill's function. In this study only the steady state force was used. Transient force development was neglected.

In the simulations the intracellular calcium $[Ca^{2+}]_i$ and stretch was set in the range 0.01 μM to 10 μM and 0.85 to 1.1, respectively. A multitude of simulations was performed varying these two parameters (Fig. 10) delivering steady forces after a transient phase. Only the steady forces were collected as results of the simulations.

The results with the two models are given in Fig. 11 b and c. The results show that both models are capable of reconstructing the steady state interdependencies between sarcomere length, intracellular calcium $[Ca^{2+}]_i$, and tension. Particularly, the steep calcium-tension relation is obvious as in measurement data. Related to the steady state stretch are characteristic changes of the half activation point, maximal force, and steepness.

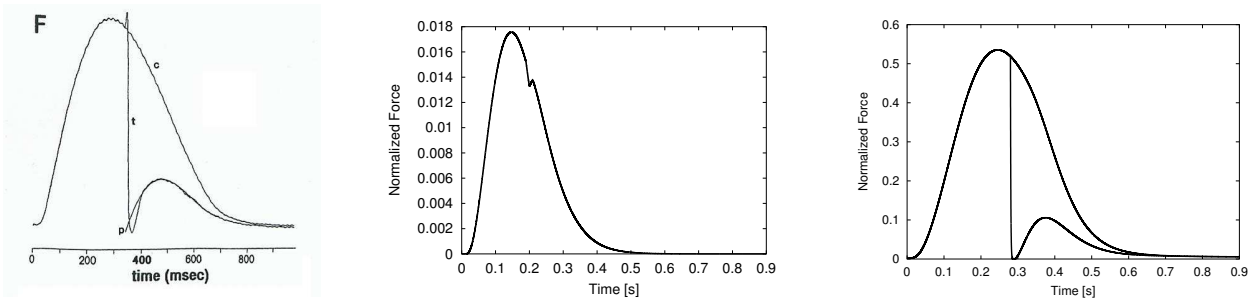

(a) (b) (c)

Figure 12. Normalized force development in length switch experiments. Force is quantified by (a) an experimental study from Peterson et al. (adapted from [Peterson et al., 1991]), (b) the 3rd Rice-Winslow-Hunter model [Rice et al., 1999], and (c) the hybrid model. The force development is shown with and without a length switch.

6.2. Simulation of length switch experiments

Length switch experiments show the influence of suddenly given displacements on the developed tension. Simulations with the 3rd Rice-Winslow-Hunter and the hybrid model were performed to reconstruct the measurements described in [Peterson et al., 1991]. The force models were coupled with the electrophysiologic cell model described in [Noble et al., 1998], which delivers an appropriate intracellular calcium transient.

In the measurement and simulations the length was fixed to the resting length with the exception of a displacement impulse, which was initiated in the descending limb of force development at time $340\ ms$. The impulse was triangle-shaped with a maximum at $95\ \%$ of resting length. $10\ ms$ were chosen for each stretch and release.

The results of the experimental study and the simulations with the models are given in Fig. 12. The results show that both models can reconstruct the steady state experiment. Only a minor decrease in tension by a length switch is determined with the 3rd Rice-Winslow-Hunter model. The hybrid model describes quantitatively appropriate the strong decrease in tension resulting from the length switch.

7. Discussion and Conclusions

A hybrid model of cardiac tension development was presented, which is derived from measurements and descriptions of the protein interactions. The model is described by a set of coupled differential equations of first order. In comparison to many other models of cardiac force development the description of the hybrid model includes detailed information concerning the binding state and configuration of the involved proteins, i.e. troponin, tropomyosin, actin, and myosin, as well as of metabolism, i.e. ATP hydrolysis. This information may be of interest to elucidate cooperativity mechanisms, pathophysiological changes, and mechano-electrical feedback mechanisms.

Results of numerical simulations with the hybrid model showed quantitative agreement with experimental studies. The results indicate that the reproduction of length switch experiments necessitates an appropriate description of the breakup of cross-bridges of actin and myosin . A description of this breakup can be achieved by velocity dependent transitions to states, where myosin is not attached to actin, i.e. M, $M \bullet ADP$, $M \bullet ATP$, and $M \bullet ADP \bullet P_i$. These transitions and states are included in the hybrid model. In simulations of normal physiology these transitions and states are not of significant importance.

Of importance for further developments will be the tissue and species specific parametrization of the hybrid model. The coupling mechanisms to electrophysiologic models can be refined, e.g. the calcium binding of troponin of the models can be unified. In conjuction with a model of cellular electrophysiology and of passive mechanics of myocardium a closed model of cardiac electromechanics can be created.

8. Appendix

8.1. Detailed description of hybrid model

Constants

$$k_{on} = 40.0\,\mu M^{-1}s^{-1} \quad (16)$$
$$k_{off} = 40.0\,s^{-1} \quad (17)$$

$$tm_{on} = 12.0\,s^{-1} \quad (18)$$
$$tm_{off} = 35.0\,s^{-1} \quad (19)$$
$$TMon_{coop} = 2.0 \quad (20)$$
$$TMon_{pow} = 2.0 \quad (21)$$

$$k_1 = 1000.0\ s^{-1} \quad (22)$$
$$k_{-1} = 10.0\ s^{-1} \quad (23)$$
$$k_2 = 1000.0\ s^{-1} \quad (24)$$
$$k_3 = 150.0\ s^{-1} \quad (25)$$
$$k_{-3} = 15.0\ s^{-1} \quad (26)$$
$$k_4 = 1500.0\ s^{-1} \quad (27)$$
$$k_{-4} = 1000.0\ s^{-1} \quad (28)$$
$$k_5 = 25.0\ s^{-1} \quad (29)$$
$$k_{-5} = 8.0\ s^{-1} \quad (30)$$
$$k_6 = 50.0\ s^{-1} \quad (31)$$
$$k_{-6} = 20.0\ s^{-1} \quad (32)$$
$$k_7 = 30.0\ s^{-1} \quad (33)$$
$$k_8 = 200.0\ s^{-1} \quad (34)$$
$$k_{-8} = 5.0\ s^{-1} \quad (35)$$
$$k_9 = 1000.0\ s^{-1} \quad (36)$$
$$k_{10} = 1000.0\ s^{-1} \quad (37)$$
$$k_{11} = 1000.0\ s^{-1} \quad (38)$$
$$k_{12} = 50.0\ s^{-1} \quad (39)$$
$$k_{13} = 1000.0\ s^{-1} \quad (40)$$
$$k_{14} = 1000.0\ s^{-1} \quad (41)$$
$$F_{max} = 0.498 \quad (42)$$
$$N_v = 10.0 \quad (43)$$
$$v50 = 3.0\ m\ s^{-1} \quad (44)$$
$$TCa_\lambda = 1.0 \quad (45)$$
$$k5_\lambda = 1.0 \quad (46)$$
$$k5_{xb} = 1.5 \quad (47)$$
$$ATP = 4.0 \quad (48)$$
$$k7_\lambda = 1.25 \quad (49)$$
$$k7_{force} = 1.0 \quad (50)$$
$$k7_{base} = 2.25 \quad (51)$$
$$v_{detach} = 10 \quad (52)$$

Initial values of state variables

$$
\begin{aligned}
T &= 1.0 && (53)\\
TCa &= 0.0 && (54)\\
TM_{off} &= 1.0 && (55)\\
TM_{on} &= 0.0 && (56)\\
M \bullet ATP &= 0.0385 && (57)\\
M \bullet ADP \bullet P_i &= 0.3846 && (58)\\
A \sim M \bullet ADP \bullet P_i &= 0.5769 && (59)\\
A \bullet M \bullet ADP \bullet P_i &= 0.0 && (60)\\
A \bullet M^* \bullet ADP &= 0.0 && (61)\\
A \bullet M \bullet ADP &= 0.0 && (62)\\
A \bullet M &= 0.0 && (63)\\
A \sim M \bullet ATP &= 0.0 && (64)\\
M &= 0.0 && (65)\\
M \bullet ADP &= 0.0 && (66)
\end{aligned}
$$

Transition equations

$$\frac{\partial TCa}{\partial t} = k_{on}(1 + S_{A\bullet M})\lambda^{TCa_\lambda}[Ca^{2+}]_i\, T - k_{off}\, TCa \tag{67}$$

$$\frac{\partial TM_{on}}{\partial t} = tm_{on}\, TCa(1 + (TMon_{coop} + \lambda)TM_{on})^{TMon_{pow}}\, TM_{off} - tm_{off}\, TM_{on} \tag{68}$$

$$v_{factor} = \frac{|v|^{N_v}}{|v|^{N_v} + v50^{N_v}} \tag{69}$$

$$
\begin{aligned}
t_1 &= k_1\, ATPA \bullet M - k_{-1}\, A \sim M \bullet ATP && (70)\\
t_2 &= k_2\, (1 + v_{factor} v_{detach})\, A \sim M \bullet ATP && (71)\\
t_3 &= k_3\, M \bullet ATP - k_{-3}\, M \bullet ADP \bullet P_i && (72)\\
t_4 &= k_4\, M \bullet ADP \bullet P_i - k_{-4}\, (1 + v_{factor} v_{detach}) A \sim M \bullet ADP \bullet P_i && (73)\\
t_5 &= k_5\, TM_{on}(k5_\lambda\, \lambda + 0.4)(1 + k5_{xb}\, S_{A\bullet M})^2 A \sim M \bullet ADP \bullet P_i - k_{-5}\, A \bullet M \bullet ADP \bullet P_i && (74)\\
t_6 &= k_6\, A \bullet M \bullet ADP \bullet P_i - k_{-6}\, A \bullet M^* \bullet ADP && (75)\\
t_7 &= k_7\, A \bullet M^* \bullet ADP\, \frac{k7_{base} - k7_\lambda \lambda + |v|}{1 + k7_{force} F} && (76)\\
t_8 &= k_8\, A \bullet M \bullet ADP - k_{-8}\, A \bullet M && (77)\\
t_9 &= k_9\, v_{factor}\, A \bullet M && (78)\\
t_{10} &= k_{10}\, v_{factor}\, A \bullet M \bullet ADP && (79)\\
t_{11} &= k_{11}\, v_{factor}\, A^* \bullet M \bullet ADP && (80)\\
t_{12} &= k_{12}\, M \bullet ADP && (81)\\
t_{13} &= k_{13}\, v_{factor}\, A \bullet M \bullet ADP \bullet P_i && (82)\\
t_{14} &= k_{14}\, ATP\, M && (83)\\
& && (84)
\end{aligned}
$$

$$\frac{\partial M \bullet ATP}{\partial t} = t_2 - t_3 + t_{14} \quad (85)$$

$$\frac{\partial M \bullet ADP \bullet P_i}{\partial t} = t_3 - t_4 + t_{13} \quad (86)$$

$$\frac{\partial A \sim M \bullet ADP \bullet P_i}{\partial t} = t_4 - t_5 \quad (87)$$

$$\frac{\partial A \bullet M \bullet ADP \bullet P_i}{\partial t} = t_5 - t_6 - t_{13} \quad (88)$$

$$\frac{\partial A \bullet M^* \bullet ADP}{\partial t} = t_6 - t_7 - t_{11} \quad (89)$$

$$\frac{\partial A \bullet M \bullet ADP}{\partial t} = t_7 - t_8 - t_{10} \quad (90)$$

$$\frac{\partial A \bullet M}{\partial t} = t_8 - t_9 - t_1 \quad (91)$$

$$\frac{\partial A \sim M \bullet ATP}{\partial t} = t_1 - t_2 \quad (92)$$

$$\frac{\partial M}{\partial t} = t_9 + t_{12} - t_{14} \quad (93)$$

$$\frac{\partial M \bullet ADP}{\partial t} = t_{10} + t_{11} - t_{12} \quad (94)$$

8.2. Implementation

The tension development and electrophysiological model were implemented with the programming languages C++ and the development package Qt, Trolltech, Norway. The simulations were performed on a Silicon Graphics Origin 2000 compute servers with 8 processors of type MIPS R10000/200 MHz and 3.8 GB of main memory. The visualizations were carried out with gnuplot.

The Euler method was used to solve the systems of coupled differential equations of first order describing the force development and electrophysiologic model [Press et al., 1992]. A time step of $10\,\mu s$ was chosen for solving of force models, a time step of $20\,\mu s$ for the electrophysiologic model. Tabularization techniques were used to reduce computing times of the electrophysiologic model.

References

[Allen and Kurihara, 1982] Allen, D. and Kurihara, S. (1982). The effects of muscle length on intracellular calcium transients in mammalian cardiac muscle. *J. Physiol.*, 327:79–94.

[Allen et al., 2000] Allen, K., Xu, Y. Y., and Kerrick, W. G. L. (2000). Ca^{2+} measurements in skinned cardiac fibers: effects of Mg^{2+} on Ca^{2+} activation of force and fiber ATPase. *J. Appl. Physiol.*, 88:180–185.

[Baker et al., 1998] Baker, A. J., Figueredo, V. M., Keung, E. C., and Camacho, S. A. (1998). Ca^{2+} regulates the kinetics of tension development in intact cardiac muscle. *Am. J. Physiol.*, 275:H744–H750.

[Bers, 1991] Bers, D. M. (1991). *Excitation-Contraction Coupling and Cardiac Contractile Force*. Kluwer Academic Publishers, Dordrecht, Netherlands.

[Bers, 2002] Bers, D. M. (2002). Cardiac excitation-contraction coupling. *Nature*, 415:198–205.

[Bluhm et al., 2000] Bluhm, W. F., Kranias, E. G., Dillmann, W. H., and Meyer, M. (2000). Phospolamban: a major determinant of the cardiac force-frequency relationship. *Am. J. Physiol.*, 278:H249–H255.

[Bluhm and Lew, 1995] Bluhm, W. F. and Lew, W. Y. W. (1995). Sarcoplasmic reticulum in cardiac length-dependent activation in rabbits. *Am. J. Physiol.*, 269(38):H965–H972.

[Bluhm et al., 1995] Bluhm, W. F., McCulloch, A. D., and Lew, W. Y. W. (1995). Active force in rabbit ventricular myocytes. *J. Biomechanics*, 28(9):1119–1122.

[Brandt et al., 1998] Brandt, P. W., Colomo, F., Piroddi, N., Poggesi, C., and Tesi, C. (1998). Force regulation by Ca^{2+} in skinned single cardiac myocytes of frog. *Biophys J*, 74:1994–2004.

[Chen et al., 2002] Chen, L. F., Winkler, H., Reedy, M. K., Reedy, M. C., and Tayler, K. A. (2002). Molecular modeling of averaged rigor crossbridges from tomograms of flight muscle. *J Struct Biol*, 138(1-2):92–104.

[de Clerck et al., 1977] de Clerck, N. M., Claes, V. A., and Brutsaert, D. L. (1977). Force velocity relations of single cardiac muscle cells. *J. Gen. Physiol.*, 69:221–241.

[Eisner et al., 1984] Eisner, D. A., Lederer, W. J., and Vaughna-Jones, R. D. (1984). The quantitative relationship between twitch tension and intracellular sodium activity in sheep cardiac Purkinje fibers. *J. Physiol.*, 355:251–266.

[Fabiato and Fabiato, 1975] Fabiato, A. and Fabiato, F. (1975). Contractions induced by a calcium-triggered release of calcium for the sarcoplasmic reticulum of single skinned cardiac cells. *J. Physiol. Lond.*, 249:469–495.

[Fung, 1993] Fung, Y. C. (1993). *Biomechanics: Mechanical Properties of Living Tissues*. Springer, New York, Berlin, Heidelberg.

[Gannier et al., 1993] Gannier, F., Bernengo, J. C., Jacquemond, V., and Garnier, D. (1993). Measurements of sarcomere dynamics simultaneously with auxotonic force in isolated cardiac cells. *IEEE Transactions on Biomedical Engineering*, 40(12):1226–1232.

[Glänzel, 2002] Glänzel, K. (2002). Kraftentwicklung im Sarkomer unter Berücksichtigung elektromechanischer Kopplung. Diploma Thesis, Institut für Biomedizinische Technik, Universität Karlsruhe (TH).

[Goodsell, 2001] Goodsell, D. S. (2001). Protein data bank. molecule of the month: Myosin. http://www.rcsb.org/pdb/molecules/pdb18_3.html.

[Gordon et al., 2001] Gordon, A., Regnier, M., and Homsher, E. (2001). Skeletal and cardiac muscle contractile activation: Tropomyosin "rocks and rolls". *News Physiol. Sci.*, 16:49–55.

[Hill, 1938] Hill, A. V. (1938). The heat of shortening and the dynamic constants of muscle. *Proc. R. Soc. Lond.*, B126:136–195.

[Hofmann and Fuchs, 1987] Hofmann, P. and Fuchs, F. (1987). Evidence for a force-dependent component of calcium binding to cardiac troponin C. *Am. J. Physiol.*, 253:C541–C546.

[Howard, 1997] Howard, J. (1997). Molecular motors: structural adaptations to cellular functions. *Nature*, 389:561–567.

[Huxley, 1957] Huxley, A. F. (1957). Muscle structures and theories of contraction. *Prog. Biophys. and biophys. Chemistry*, 7:255–318.

[Huxley, 2001] Huxley, A. F. (2001). Cross-bridge action: present views, prospects and unknowns. *J Biomechanics*, 33:1189–1195.

[Ingebretsen et al., 1976] Ingebretsen, W. R., Becker, E., Friedman, W. F., and Mayer, S. E. (1976). Contractile and biochemical responses of cardiac and skeletal muscle to isoproterenol covalently linked to glass beads. *Circ. Res.*, 40(5):474–484.

[Irving and Goldman, 1999] Irving, M. and Goldman, Y. E. (1999). Another step ahead for myosin. *Nature*, 398:463–465.

[Janssen and de Tombe, 1997] Janssen, P. M. L. and de Tombe, P. P. (1997). Uncontrolled sarcomere shortening increases the intracellular Ca^{2+} transient in rat cardiac trabeculae. *Am. J. Physiol.*, 272:H1892–H1897.

[Janssen and Hunter, 1995] Janssen, P. M. L. and Hunter, W. C. (1995). Force, not sarcomere length, correlates with prolongation of isosarcometric contaction. *Am. J. Physiol.*, 269:H676–H685.

[Kentish et al., 1986] Kentish, J. C., ter Keurs, H. E., Ricciardi, L., Bucx, J. J., and Noble, M. I. (1986). Comparison between the sarcomere length-force relations of intact and skinned trabeculae from rat right ventricle. influence of calcium concentrations on these relations. *Circ. Res*, 58(6):755–68.

[Kitamura et al., 1999] Kitamura, K., Tokunaga, M., Iwane, A. H., and Yanagida, T. (1999). A single myosin head moves along an actin filament with regular steps of 5.3 nanometeres. *Nature*, 397:129–134.

[Kohl et al., 1998] Kohl, P., Day, K., and Noble, D. (1998). Cellular mechanisms of cardiac mechano-electric feedback in a mathematical model. *Can. J. Cardiol.*, 14(1):111–119.

[Konhilas et al., 2002] Konhilas, J. P., Irving, T. C., and de Tombe, P. P. (2002). Myofilament calcium sensitivity in skinned rat cardiac trabeculae - role of interfilament spacing. *Circ. Res.*, 90:59–65.

[Layland and Kentish, 1999] Layland, J. and Kentish, J. C. (1999). Positve force and $[Ca^{2+}]_i$-frequency relationships in rat ventricular trabeculae at physiological frequencies. *Am. J. Physiol.*, 276:H9–H18.

[Lodish et al., 2001] Lodish, H., Berk, A., Zipursky, S. L., Matsudaira, P., Baltimore, D., and Darneell, J. (2001). *Molekulare Zellbiologie*. Spektrum Akademischer Verlag, Heidelberg, Berlin.

[Maier et al., 2000] Maier, L. S., Barckhausen, P., Weisser, J., Aleksic, I., Baryalei, M., and Pieske, B. (2000). Ca^{2+}-handling in isolated human atrial myocardium. *Am. J. Physiol.*, 279:H952–H958.

[Maier et al., 1998] Maier, L. S., Brandes, R., Pieske, B., and Bers, D. M. (1998). Effect of left ventricular hypertrophy on force and Ca^{2+}-handling in isolated rat myocardium. *Am. J. Physiol.*, 274:H1361–H1370.

[Moss et al., 1986] Moss, R., Allen, J., and Greaser, M. (1986). Effecs of partial extraction of troponin complex upon the tension-pCa relation in rabbit skeletal muscle. *J. Gen. Physiol*, 87:761–774.

[Nagashima and Asakura, 1982] Nagashima, H. and Asakura, S. (1982). Studies on co-operative properties of tropomyosin-actin and tropomyosin-troponin-actin complexes by use of N-ethylmaleinide-treated and untreated species of myosin subfragment. *J. Mol. Bio.*, 155:409–428.

[Nassar et al., 1991] Nassar, R., Malouf, N. N., Kelly, M. B., Oakely, A. E., and Anderson, P. A. W. (1991). Force-pCa relation and troponin T isoforms of rabbit myocardium. *Circ. Res.*, 69(6):1470–1475.

[Noble et al., 1998] Noble, D., Varghese, A., Kohl, P., and Noble, P. (1998). Improved guinea-pig ventricular cell model incorporating a diadic space, I_{Kr} and I_{Ks}, and length- and tension-dependend processes. *Can. J. Cardiol.*, 14(1):123–134.

[Noble, 2000] Noble, P. (2000). -. personal communication.

[O'Rourke et al., 1999] O'Rourke, B., Kass, D. A., Tomaselli, G. F., Kaab, S., Tunin, R., and Marbán, E. (1999). Mechanisms of altered excitation-contraction coupling in canine tachycardia-induced heart failure, I experimental studies. *Circ. Res*, 84(5):562–570.

[Palmer and Kentish, 1998] Palmer, S. and Kentish, J. C. (1998). Role of Ca^{2+} and crossbridge kinetics in determining the maximum rates of Ca^{2+} activation and relaxation in rat and guinea pig skinned trabeculae. *Circ. Res.*, 83:179–186.

[Parmley and Chuck, 1973] Parmley, W. W. and Chuck, L. (1973). Length-dependent changes in myocardial contractile state. *Am. J. Physiol.*, 224(5):1195–1199.

[Peterson et al., 1991] Peterson, J. N., Hunter, W. C., and Berman, M. R. (1991). Estimated time course of Ca^{2+} bound to troponin C during relaxation in isolated cardiac muscle. *Am. J. Physiol. Circ. Heart.*, 260:H1013–H1024.

[Press et al., 1992] Press, W. H., Teukolsky, S. A., Vetterling, W. T., and Flannery, B. P. (1992). *Numerical Recipes in C*. Cambridge University Press, Cambridge, New York, Melbourne, 2 edition.

[Rice et al., 1999] Rice, J. J., Winslow, R. L., and Hunter, W. C. (1999). Comparison of putative cooperative mechanisms in cardiac muscle: length dependence and dynamic responses. *Am. J. Physiol. Circ. Heart.*, 276:H1734–H1754.

[Sachse, 2002] Sachse, F. B. (2002). Modeling of the mammalian heart. Universität Karlsruhe (TH), Institut für Biomedizinische Technik. Habilitationsschrift.

[Saeki et al., 1998] Saeki, Y., Kurihara, S., Komukai, K., Ishikawa, T., and Takigiku, K. (1998). Dynamic relations among length, tension, and intracellular Ca^{2+} in activated ferret papillary muscles. *Am. J. Physiol.*, 275:H1957–H1962.

[Sonnenblick, 1964] Sonnenblick, E. H. (1964). Series elastic and contractile elements in heart muscles: changes in muscle length. *Am. J. Physiol.*, 207(6):1330–1338.

[Spudich, 2001] Spudich, J. A. (2001). TIMELINE: The myosin swinging cross-bridge model. *Nature Reviews Molecular Cell Biology*, 2:387–392.

[Swartz and Moss, 1992] Swartz, D. and Moss, R. (1992). Influence of a strong-binding myosin analoque on calcium-sensitive mechanical properties of skinned skeletal muscle fibers. *J. Biol. Chem.*, 267:20497–20506.

[ter Keurs et al., 2000] ter Keurs, H. E. D. J., Hollander, E. H., and ter Keurs, M. H. C. (2000). The effect of sarcomere length on the force-cytosolic $[Ca^{2+}]$ relationship in intact rat cardiac trabeculae. In Herzog, W., editor, *Skeletal muscle mechanics: From Mechanisms to Function*, chapter 4, pages 53–70. John Wiley & Sons, Ltd, Baffins Lane, Chichester, West Sussex P019 1UD, UK.

[Tobacman, 1996] Tobacman, L. (1996). Thin filament mediated regulation of cardiac contraction. *Ann. Rev. Physiol.*, 58:447–481.

[Wang and Patterson, 1995] Wang, L. and Patterson, R. (1995). Multiple sources of the impedance cardiogram based on 3-d finite difference human thorax models. *IEEE Transactions on Biomedical Engineering*, 42(2):141–148.

[Wannenburg et al., 2000] Wannenburg, T., Heijne, G. H., Geerdink, J. H., van den Dool, H. W., Janssen, P. M. L., and de Tombe, P. P. (2000). Cross-bridge kinetics in rat myocardium: effect of sarcomere length and calcium activation. *Am. J. Physiol.*, 279:H779–H790.

[White et al., 1995] White, E., Boyett, M. R., and Orchard, C. H. (1995). The effects of mechanical loading and changes to length on single guinea-pig ventricular myocytes. *J. Physiol.*, pages 93–107.

[White et al., 1993] White, E., Guennec, J.-Y. L., Nigretto, J. M., Gannier, F., Argibay, J. A., and Garnier, D. (1993). The effects of increasing cell length on auxotonic contractions; membrane potential and intracellular calcium transients in single guinea-pig ventricular myocytes. *Experimental Physiol.*, pages 65–78.

[Wier and Yue, 1986] Wier, W. G. and Yue, D. T. (1986). Intracellular calcium transients underlying the short-term force-interval relationship in ferret ventricular myocardium. *J. Physiol.*, 376:507–530.

[Yasuda et al., 2001] Yasuda, S., Sugiura, S., Kobayakawa, N., Fjita, H., Yamashita, H., Katoh, K., Seaki, Y., Kaneko, H., Suda, Y., Nagai, R., and Sugi, H. (2001). A novel method to study contraction characteristics of a single cardiac myocyte using carbon fibers. *Am. J. Physiol.*, 281:H1442–H1446.